Magnetostatic Cleanliness of the Radioistope Thermoelectric Generators (RTGs) of Cassini

P. Narvaez - Jet Propulsion Laboratory, California Institute of Technology
K. Mehlem - ESA-ESTEC, 2200 AG Noordwijk, The Netherlands

Abstract. The Cassini spacecraft, launched on October 1997 to reach Saturn in 2004, carries two magnetometer experiments at the end of a 10-meter boom. In order to gather valid scientific magnetic field data and avoid electromagnetic interference, the spacecraft had to comply with a stringent magnetostatic cleanliness requirement. Amidst the strongest magnetic field perturbations were three Radioisotope Thermoelectric Generators (RTGs), which provide power to the spacecraft's multiple number of engineering and science instruments. The RTGs (Figure 1) have been compensated efficiently. This paper describes the field-mapping technique, the numerical modeling and the compensation approach used for the RTGs with the goal of minimizing its magnetic field interference with Cassini's DC magnetic field science instruments. The overall cleanliness results of Cassini will also be presented.

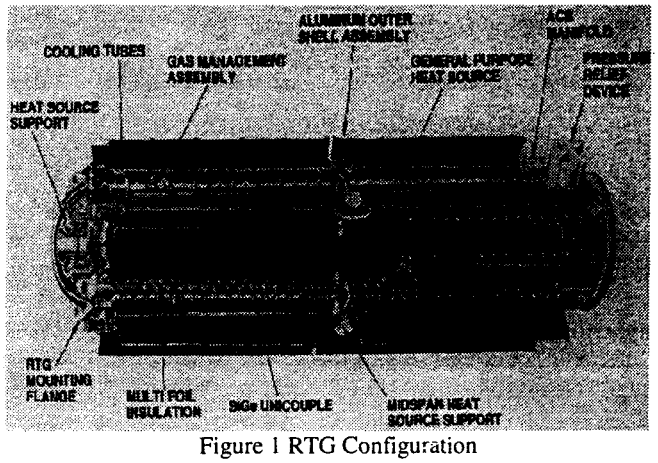

Figure 1 RTG Configuration

INTRODUCTION

Numerous scientific spacecraft such as the Pioneers, the Voyagers, Galileo, Ulysses and Cassini carry highly sensitive magnetometer experiments for measuring planetary and interplanetary magnetic fields. The magnetic fields to be measured are in the range of a few nanoTeslas (nT) up to the full planetary near-field strength in the order of 105 nT or 1 Gauss. In order to avoid interference with the magnetometers, the scientific requirements imposed on a spacecraft very stringent magnetic cleanliness levels as low as 0.1 nT at the magnetometer experiment location. Since a spacecraft contains unavoidably a number of magnetic sources such as motors, magnetic materials and current loops, a series of measures have to be taken to reduce the magnetic interference affecting the measurements during operation. These measures constitute the Magnetic Cleanliness Program. One effective measure to achieve a reduction of the spacecraft field is to place the magnetometer sensor at the tip of a long boom, which can be up to 10 meters in length. Other measures include following specific designs of spacecraft payload components such as the minimization of current loops in printed circuit boards, choosing non-magnetic materials, the magnetic compensation of critical units using compensation magnets, the avoidance of accidental magnetization (perm) etc. In addition, all magnetic units and subsystems are tested in coil facilities by measuring their respective near-field DC magnetic field signature and are demagnetized wherever possible and necessary. The success of all these activities of the Magnetic Cleanliness Program is normally verified in a final test of the fully integrated spacecraft. Unfortunately, when the magnetometer boom is deployed, the spacecraft usually is too large to fit into even the largest magnetic test facilities available today; moreover, no present day facility can verify experimentally the cleanliness level of a spacecraft to 0.1 nT since test equipment resolution is typically only > 0.5 nT. Deriving numerical models of the magnetic sources on the basis of multiple spacecraft component level near-field measurements (signal-to-noise-ratio > 10) circumvents this handicap. These models then allow computing precisely the far-fields at the magnetometer experiment sensor location. Cassini has a cleanliness specification of < 0.2 nT. It contains a number of highly magnetic units like its three RTGs which, taken together, would consume the total allowable cleanliness allocation for the spacecraft. The RTGs, despite a very careful self-compensating harness routing within its design, emit residual electro-magnetic fields which amount to 40% of the total overall s/c allowable field at the outboard magnetometer sensor location. For evident health and safety reasons these RTGs, fueled with radioactive material, could not be easily transported to a magnetic facility with a Helmholtz coil testing system. Such a system, which shields the test item from interacting with the Earth's field, is required for performing DC magnetic field testing with accuracies of +/-1 nT. However, in the case of the RTGs, the challenge was to test in the presence of the Earth's magnetic field and still maintain an accuracy of +/- 1 nT in the presence of the ambient magnetic field. The measurements had to be made in the Earth's-field and with nearby disturbances created by the industrial environment at the EG&G plant in Miamisburg, Ohio. This paper describes in some detail how these RTGs have been measured, modeled and compensated under particularly unfavorable circumstances, requiring special modeling and compensation methods. A short synthesis of the total spacecraft cleanliness level is also given and compared to preliminary flight data.

DATA ACQUISITION

All four Cassini RTGs, three flight units and a single spare unit, were tested at EG&Gís Mound Laboratories located in Miamisburg, Ohio. Data was acquired using a data acquisition system designed by Mound Laboratories. Tests were performed at the magnetic test facility located in Cell 110 of Building 50. Cell 110 featured a non-magnetic, remote-rotatable table and a non-magnetic RTG "A" frame holding fixture. Via a drive shaft system the table is rotated automatically and an encoder underneath the table was set to make field readings every 10 degrees. Since radiation was a major concern during the RTG tests due to the high neutron and gamma radiation dose rates in proximity to the fueled RTG, only the required personnel were permitted in the immediate work areas. The test chamber used for testing the RTGs had reinforced concrete walls of 1 meters thick. A layout of the facility is shown in Figure 2.

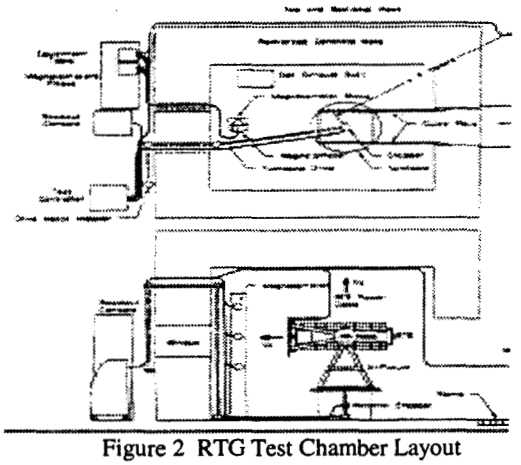

Figure 2 RTG Test Chamber Layout

During the tests, personnel were required to maintain as much separation from the RTG as was reasonable. Furthermore, due to the high RTG temperature (about 245 C on fin surface), test personnel were forced to observe extreme care that no bare skin came in contact with the RTGs. All test operators entering the cell during the calibration phase or actual magnetic field measurements were required to be free of any ferrous items such as wrist watches, belt buckles etc. The RTG was carefully moved from its service chamber and into the test area by using a crane and forklift.

Three 3-axes magnetometer sensors for a total of nine sensor elements were used to measure the RTG magnetic field signature. One 3-axes magnetometer cluster, identified as Sensor 2, was aligned on axis with the radial RTG axis while the other two 3-axes magnetometer sensors, identified as Sensor 1 and Sensor 3, were placed 30 degrees above and below the RTG plane, respectively. Each sensor element was positioned 1.5 meters from the geometric center of the RTG. An accurately scribed steel bar was used to line up all sensors to 1.5 meters. A laser was then used to verify the proper location of the horizontal centerline of Sensor 2. Within the magnetometer sensor elements, the Sensor 1 elements were identified as elements 1X, 1Y and 1Z, while Sensor 2 elements were identified as elements 2X, 2Y and 2Z, and finally, Sensor 3 elements were identified as elements 3X, 3 Y and 3Z, respectively. The overall test set up is shown in Figure 3.

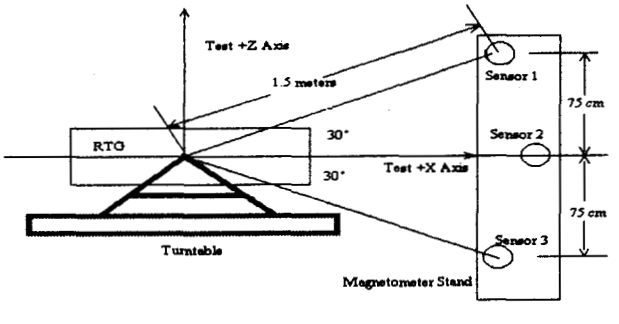

Figure 3 RTG Test Configuration and Orientation

JPL provided the measurements equipment, including the nine magnetometer sensors needed. And ESA/ESTEC provided the analytical software programs, which were used in reducing the raw data. EG&G Mound Labs provided the data acquisition system which took analog readings from the magnetometer sensor electronics and digitized the measured field data and provided output files of all measured raw data.

Prior to introducing the RTG into the test chamber, all nine magnetometer probe elements were adjusted to produce a zero magnetic field reference. Final zero-field adjustments were performed under controlled and magnetically stable conditions. Vehicle activity outside building was not permitted and all building doors were guarded shut to minimize disruption of zero-field stability. For this reason, tests were performed starting at midnight. Once the zero-reference field was accepted, a test calibration coil with a known theoretical magnetic field was tested to validate the overall test set-up. In this manner, all nine magnetometer sensors were checked against known theoretical results. An accurate DC current from a calibrated current source was applied to the calibration coil.

An ambient magnetic field characterization was then performed. The turntable with no RTG in Cell 110 was rotated through 5 consecutive rotations and magnetic fields were recorded at 10 degrees steps in a counter clockwise rotation. This verified that a zero field output was obtained on all nine sensor elements. A typical output consisted of nine straight field signatures near the zero field mark.

Next, a dry run was performed with a calibration coil in two positions. Readings were obtained at 10 degree steps in a counterclockwise rotations. Results were compared to theoretical predictions in order to ensure that the test chamber was not introducing distortions in magnetic fields within the chamber. Results indicated satisfactory conditions. Sensor elements 1X, 1Y, 2X, 2Y, 3X and 3Y all showed the expected sinusoidal magnetic field signature typical of a pure dipolar source. Sensor elements 1Z, 2Z and 3Z produced straight-line elements as expected. After all nine sensor elements were satisfactorily compared to theoretical results, the test chamber and test equipment set-up was validated for the RTG test. After these series of validation tests, the RTG was ready for test.

Magnetic field measurements were performed on all four of the Cassini RTGs at different periods from September 1995 through January 1997. It was predicted, based on the inherent current loop in the RTG wiring design, that the four RTGs would produce the most significant dipole magnetic moment sources on the Cassini spacecraft. In order to reduce their collective magnetic cleanliness effect on the magnetometer science, it was determined that the best field cancellation approach would be to use the respective RTG dipole moment components to cancel each other out. Clocking angles were chosen which produced the best positions and clocking to minimize magnetic fields at the VHM. Before all this could be made possible, each RTG had to be precisely measured to within +/- 1 nT in a hostile test environment.

The RTG was mapped at ten-degree increments of rotation. Magnetic mapping was done about both the vertical Y-axis and about the vertical Z-axis. The RTG was mapped until a stable current was achieved. The RTG was held by a gimbal for rotation around the RTGs longitudinal axis; the gimbal was placed on a turntable. By using the gimbal the RTG was able to be measured in the horizontal and in the vertical plane. Each complete run (2 planes) produces 216 field vectors, and the measurements were repeated up to five times for averaging out of measurement errors.

DATA ANALYSIS

As mentioned above it is impossible in most cases to verify the magnetostatic cleanliness level at the spacecraft sensor directly by measurements in the laboratory. The purpose of magnetostatic modeling is therefore to circumvent this handicap by deriving Multiple Dipole Models (MDMs) on the basis of near-field measurements (signal-to-noise ratio > 10) and to predict the field at the sensor location (far-field) accurately.

MDM Method

The MDM method is based on the postulate that any field configuration can be explained by a final set of n_d dipoles (positions and moments) located within the test object. The method consists therefore of the determination of these multiple dipole models (MDMs) which can then be used to predict accurately the field at distances greater than the measurement distance. In addition, allow some physical interpretation of the magnetic sources inside the test object. The so defined model-parameter identification problem is solved by use of a classical Nonlinear Programming (NLP) method as described hereafter. In contrast to the Spherical Harmonic Analysis, which require more elaborate scanning techniques and which produces more abstract results in the form of the spherical coefficients, the MDM method uses single-plane, and exceptionally dual-plane rotational measurement techniques. The test object is placed on a turntable. The turntable is rotated counter-clockwise by n_a (36) equal angular rotational steps. n_s tri-axial sensors containing n_e (3) orthogonal sensor elements, are distributed vertically at one side of the turntable in such a way that the test object is covered optimally. At each rotational step the sensors measure the field vectors generated by the test object.

Now the main question arises: How can we determine the optimal positions $\mathbf{p}_l$ and moments $\mathbf{m}_l$ of a MDM (for a given number of dipoles n_d) that minimize the difference between the measured and the calculated field vectors in the sense of a least squares fit?

Optimal Dipole Moments

Let:

$\mathbf{r}_i$	= sensor positions vector	$i=1,n_s$	(3x1)
$\mathbf{b}^m_{ij}$	= measured field vector	$i=1,n_s$; $j=1,n_a$	(3x1)
$\mathbf{b}^c_{ij}$	= calculated field vector	$i=1,n_s$; $j=1,n_a$	(3x1)
$\mathbf{p}_l$	= dipole positions vector	$l=1,n_d$	(3x1)
$\mathbf{m}_l$	= dipole moments vector	$l=1,n_d$	(3x1)

The calculated field vector $\mathbf{b}^c_{ij}$ generated by n_d dip8oles $\mathbf{m}_l$ at the rotational step j and at the sensor i is:

$$\mathbf{b}^c_{ij} = \sum_{l=1}^{n_d} \mathbf{G}_{ijl}\ \mathbf{R}_j\ \mathbf{m}_l \quad \{i=1,n_s;\ j=1,n_a\}$$

with the "geometrical" (3x3) matrix $\mathbf{G}_{ijl}$ containing the cubic law:

$$\mathbf{G}_{ijl} = (3\mathbf{q}_{ijl}^T\,\mathbf{q}_{ijl} - \mathbf{I}) / |\mathbf{d}_{ijl}|^3 \qquad (3x3)$$

where $\mathbf{q}_{ijl} = \mathbf{d}_{ijl} / |\mathbf{d}_{ijl}|$ and $\mathbf{d}_{ijl} = \mathbf{r}_i - \mathbf{R}_j\,\mathbf{p}_l$

$\mathbf{R}_j$ is the (3x3) rotation matrix for the rotation around the vertical axis.

Let us collect all the measured field vectors $\mathbf{b}^m_{ij}$ in a large array $\boldsymbol{b}^m$ and all the calculated field vectors $\mathbf{b}^c_{ij}$ in a large array $\boldsymbol{b}^c$, both of dimension ($[n_s n_a n_e]$ x 1), such that the index q of element b_q is defined by $q = n_a n_e(i-1) + n_e(j-1) + k$. Let us also collect all the dipole position vectors $\mathbf{p}_l$ in a large array $\boldsymbol{p}$ and the all the dipole moment vectors $\mathbf{m}_l$ in a large array $\boldsymbol{m}$, both of dimension ($[3n_d]$ x 1), such that the index t of element p_t and m_t is defined by $t = 3n_d(l-1) + k$. Then we can write the condensed equation for the calculated field $\boldsymbol{b}^c$:

$$\boldsymbol{b}^c = \boldsymbol{G}\,\boldsymbol{m}$$

with the ($n_s n_a n_e$ x $3n_d$) matrix $\boldsymbol{G}$ containing the (3x3) blocks:

$$\boldsymbol{G}_{ul} = \mathbf{G}_{ijl} \quad \{u = n_a(i-1) + j;\ \ i=1,n_s;\ \ j=1,n_a;\ \ l=1,n_d\}$$

With a suitable choice of the test-setup geometry (number of sensors n_s, location of sensors $\mathbf{r}_j$ and number of rotational steps n_a) it is always possible to ensure that $\boldsymbol{G}$ is well conditioned.

Replacing $\boldsymbol{b}^c$ by $\boldsymbol{b}^m$ and solving the linear equation of $\boldsymbol{b}^m = \boldsymbol{G}\,\boldsymbol{m}$ for $\boldsymbol{m}$ we can find the optimal dipole moments $\boldsymbol{m}^*(\boldsymbol{p})$ in the sense of least squares:

$$\boldsymbol{m}^* = \boldsymbol{G}^+\,\boldsymbol{b}^m = (\boldsymbol{G}^T\boldsymbol{G})^{-1}\boldsymbol{G}^T\,\boldsymbol{b}^m$$

where $\boldsymbol{G}^+ = (\boldsymbol{G}^T\boldsymbol{G})^{-1}\boldsymbol{G}^T$ is the generalized inverse of $\boldsymbol{G}$.

Replacing $\boldsymbol{m}^*(\boldsymbol{p})$ in the eq. for $\boldsymbol{b}^c$ we get the least square solution $\boldsymbol{b}^{c*}(\boldsymbol{p})$:

$$\boldsymbol{b}^{c*} = \boldsymbol{G}\,\boldsymbol{m}^* = \boldsymbol{G}\,\boldsymbol{G}^+\,\boldsymbol{b}^m = \boldsymbol{G}\,(\boldsymbol{G}^T\boldsymbol{G})^{-1}\boldsymbol{G}^T\,\boldsymbol{b}^m$$

Optimal Dipole Positions

Let the quadratic cost function c as a function of $\boldsymbol{p}$ be:

$$c(\boldsymbol{p}) = \mathbf{e}(\boldsymbol{p})^T\mathbf{e}(\boldsymbol{p})$$

The optimality condition is $c_{min}(\boldsymbol{p}^{opt}) \le c(\boldsymbol{p}) \quad \forall\ \boldsymbol{p} \in R^n$

The ($n_s n_a n_e$ x 1) field mis-modeling vector $\mathbf{e}(\boldsymbol{p})$ is defined by:

$$\mathbf{e} = \boldsymbol{b}^{c*} - \boldsymbol{b}^m = \{\boldsymbol{G}\,(\boldsymbol{G}^T\boldsymbol{G})^{-1}\boldsymbol{G}^T - \boldsymbol{I}\}\,\boldsymbol{b}^m$$

The ($n_s n_a n_e$ x1) derivative vector $\mathbf{c}'(\boldsymbol{p})$ is:

$$\mathbf{c}' = \delta c / \delta \boldsymbol{p} = 2(\delta \mathbf{e} / \delta \boldsymbol{p})^T\,\mathbf{e} = 2\mathbf{S}^T\mathbf{e}$$

where $\mathbf{S}$ is the ($n_s n_a n_e$ x $3n_d$) sensitivity matrix. The derivatives are approximated by one-sided finite perturbations of the parameters p_t.

The ($n_s n_a n_e$ x $n_s n_a n_e$) second derivative Hessian matrix $\mathbf{C}''$ is:

$$\mathbf{C}'' = 2\mathbf{S}^T\mathbf{S} + 2(\delta^2\mathbf{e} / \delta \boldsymbol{p}^2)^T\mathbf{e}$$

The second term $2(\delta^2\mathbf{e} / \delta \boldsymbol{p}^2)^T\mathbf{e}$ contains second derivatives; it vanishes for $\mathbf{e} \to \mathbf{0}$ in the vicinity of the optimum $c_{min}(\boldsymbol{p}^{opt})$. We therefore retain only the approximated Hessian matrix $\mathbf{H} = 2\mathbf{S}^T\mathbf{S}$.

With a suitable choice of the MDM configuration (number n_d and position $\mathbf{p}_l$ of the dipoles) it is always possible to ensure that $\boldsymbol{H}$ is well conditioned.

The Gauss-Newton algorithm for the iterative search of $\boldsymbol{p}$ can now be written:

$$\boldsymbol{p}^+ = \boldsymbol{p} + f_0\,[\mathbf{H}]^{-1}\,\mathbf{c}' = \boldsymbol{p} + f\,[\mathbf{S}^T\mathbf{S}]^{-1}\,\mathbf{S}^T\mathbf{e} = \boldsymbol{p} + f\,\mathbf{S}^+\mathbf{e}$$

The second term can be interpreted as the search direction $\mathbf{u} = \mathbf{S}^{+}\mathbf{e}$, multiplied by the progress factor f which is determined by a sub-procedure which leads to the local minimum $c(\boldsymbol{p}_{l+1})$ on $\mathbf{u}$. For f we use the Fibonacci sequence up to order 5 followed by a final cubic interpolation. The stop criteria of the main iteration process are:

$$c(\boldsymbol{p}^{+}) < \varepsilon_1 \text{ or } |c(\boldsymbol{p}^{+}) - c(\boldsymbol{p})| < \varepsilon_2 \text{ or } |\mathbf{c}'(\boldsymbol{p}^{+})| < \varepsilon_3$$

The algorithm is characterized by a large convergence domain, by a superlinear convergence rate, by the need for only first derivatives and by a second derivative matrix $\mathbf{H}$ semi-definit positive by construction. Unfortunately a unique MDM solution does not exist. For different numbers of dipoles n_d different optimal MDMs can be found leading to a given level of acceptable field residues $c(\boldsymbol{p})_{low.lim}$. For far-fields where the test object appears as a dipole n_d=1 is the minimum value; n_d>1 would lead to over-parametrization. $n_{d.min}$ is clearly a function of the test distance and has therefore to be determined by varying n_d=1,2,3,$n_{d.min}$. The lower the test distance the higher is $n_{d.min}$ and the better the MDM describes discrete magnetic sources within the test object. An example for determining $n_{d.min}$ will be given in the next section. It can happen that during the iteration process two dipole positions converge. In this case $\mathbf{S}$ is not of full rank any more and the search direction $\mathbf{u}$ is perpendicular to the gradient $\mathbf{c}'$. A practical method to reestablish convergence, is to define a new search direction
$\mathbf{u}^{+} = (\mathbf{u} - \mathbf{c}')/2$; a step in this new direction would separate the dipoles and lead to a lower cost function. In many cases this situation occurs when the MDM is over-parametrized or when the measurements are not coherent with any non-pathological MDM. Since no constraints on $\boldsymbol{p}$ are allowed it can also happen that $\boldsymbol{p}$ wants to exceed the physical boundaries of the test object. This indicates usually that there are some inconsistencies in the measurements $\boldsymbol{b}^{m}$.

The main result of the optimization is the couple
$\{\boldsymbol{p}^{opt}, \boldsymbol{m}^{*}(\boldsymbol{p}^{opt})\} = \{\boldsymbol{p}, \boldsymbol{m}\}^{opt}$ which represents the optimal MDM.

RTG Data Analysis

RTG Data Correction.

In order to reduce the influence of measurement noise 5 to 10 rotational measurements were taken. In the previous section it had been assumed that the measurements $\boldsymbol{b}^{m}$ do not contain any bias. Unfortunately, the repeated RTG measurements showed some random constant biases, as shown in Figure 4. Therefore the average field, which was used for modeling, was biased too. These biases were probably due to the environment of the EG&G site and to the magnetometer electronics.

Evidently, these biases lead to wrong MDMs. Therefore the method had to be modified. The solution to the problem comes from the fact that, according to theory (div$\mathbf{b}$ = 0), the integral of the field in direction of and along a closed path must be zero. This is precisely the case for the lateral (tangential) or y-component (k=2). Using the div$\mathbf{b}$=0 condition, the bias of the y-component is eliminated by:

$$b^{m.corr}_{ijk} = b^{m}_{ijk} - (1/n_a) \sum_{j=1}^{n_a} b^{m}_{ijk} \qquad \{i=1,n_s\ ;\ j=1,n_a\ ;\ k=2\}$$

However, in a single-plane rotational mode, the MDM would still be undetermined because no unbiased vertical component is available. Fortunately, the RTG test fixture allowed for a rotation of the RTG around its longitudinal axis, as shown on the Figure ???. By rotating the RTG's z-axis counterclockwise by 90° around its longitudinal (x-) axis into the x,y-plane, a second field data set was obtained, which contained also information about the RTG's vertical component. With this corrected y-component a MDM and the field $\mathbf{b}^{c}_{ijk}$ is calculated. Furthermore, by a special formulation, it was now also possible to use the biased x- and z- components as well. For this, the measured x- and z-components were corrected by the average of the calculated x- and z-components:

$$b^{m.corr}_{ijk} = b^{m}_{ijk} - (1/n_a) \sum_{j=1}^{n_a} b^{c}_{ijk} \qquad \{i=1,n_s\ ;\ j=1,n_a\ ;\ k=1,n_c;\ k \neq 2\}$$

This was repeated at each step of the iterations. In this way, a best fit was obtained (see Figure 6). Also, as a side result a good estimate of the biases was obtained by $b^{bias}_{ijk} = b^{m}_{ijk} - b^{c}_{ijk}$.

RTG Model Validation

In the framework of Cassini a total of four RTGs had undergone magnetic testing. For each of their MDM a search had to be made for the minimal necessary number of dipoles $n_{d.min}$ as mentioned above.

In non-pathological cases the global moment $|\mathbf{m}^{g}_{nd}| = \sum_{l=1}^{n_d} \mathbf{m}_l$ converges to a limit value for increasing n_d. In the Figure 5 we compare the global moments $|\mathbf{m}^{g}_{1}|$ to $|\mathbf{m}^{g}_{5}|$ with the reference global moment $|\mathbf{m}^{g}_{6}|$. It turns out that already for $|\mathbf{m}^{g}_{2}|$ the difference is about 2% with a rms of field residues of 16%. With $|\mathbf{m}^{g}_{5}|$ the difference vanishes with a rms field residues of about 5%; this is the adopted minimum MDM. Figure 6 shows a typical optimal data fit by a 5DM.

RTG Models

All four MDMs are shown on Figure 7 in the form of the field at the test distance. Against expectation the RTGs differ significantly from each other. In particular, F6 and F7 each have a big lobe. By making measurements with the RTGs F6 and F7 in open circuit (no current flow) we could identify precisely material-magnetic sources at one end inside the RTGs (see Figure 8). Since the spacecraft is scheduled to arrive only in 2004 for Saturn Orbital Insertion (SOI), the MDMs had to be corrected for the expected loss of electrical power of the RTGs in 2004 by applying a correction factor to the dipole moments; for F6 and F7 we had first to extract numerically the material-magnetic part of the MDMs (Figure 8), correct the electromagnetic part and add both parts together again.

RTG Compensation

After having obtained all four MDMs of the RTGs, the next task was to minimize the combined field emission at the Cassini Vector Helium Magnetometer (see the RTG configuration on Figure 9) by point compensation, in contrast to the more problematic global compensation. A compensation of each individual RTG by use of magnets (as applied to the Ulysses RTG) was prohibitive due to the extra amount of testing and due to the extra exposure to radiation of the test personnel. Two circumstances helped us. Firstly, the global moment of each RTG showed a strong non-axial component. Secondly, the project allowed us to chose the positions (see Figure 9) and the clocking angles (angular position around the longitudinal axis) of the RTGs. The allowed clocking angles were every 30° but some of them were prohibited. By simulation it could be shown that self-compensation by optimal choice of positions and clocking angles existed (see Figure 10). By a search of all possible configurations a solution was retained which minimizes the field at the Vector Helium Magnetometer (VHM). The results are shown in the following table:

Position		1	2	3	b_{FGM} (pT)	b_{VHM} (pT)
RTG	optimal	F6	F2	F7		
Clocking Angle	nominal	0	0	0	311	49
	optimal	-120	90	-60	56	4

These values had been accepted by the Cassini project and the integration of the RTGs on the spacecraft was done accordingly (see Figure 9). Figure 11 illustrates the strong compensation involved. Figure 12 shows the field $|\mathbf{b}^c|$ over the x_s,y_s-plane of the spacecraft containing the FGM and the VHM location and it illustrates the achieved compensation.

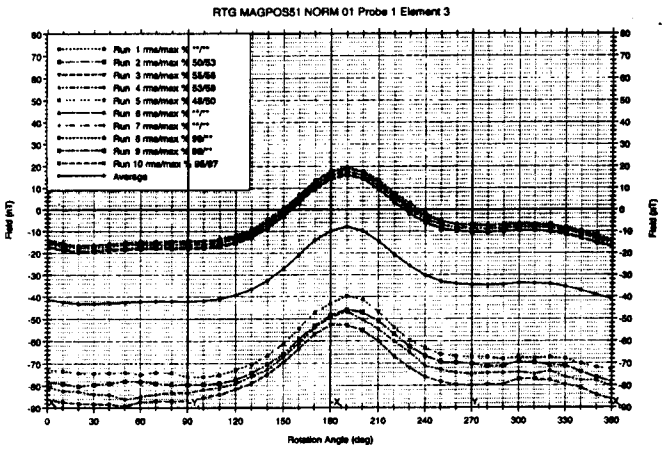

Figure 4

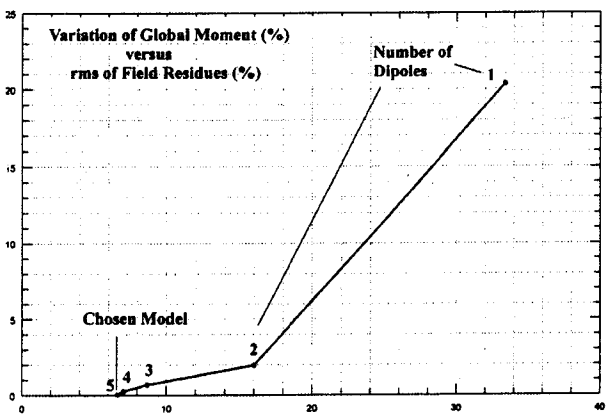

Figure 5

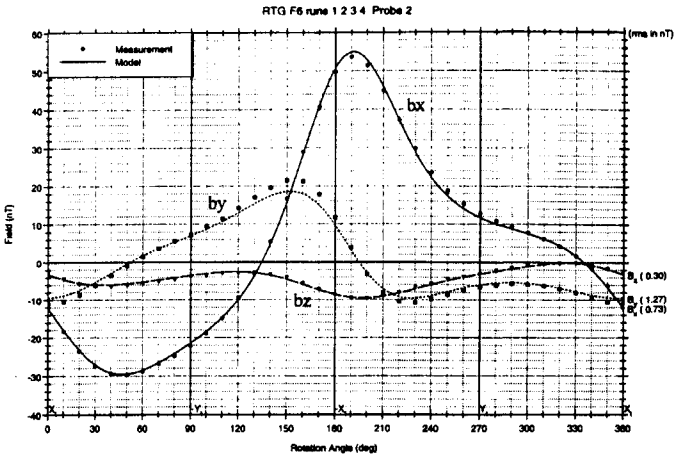

Figure 6

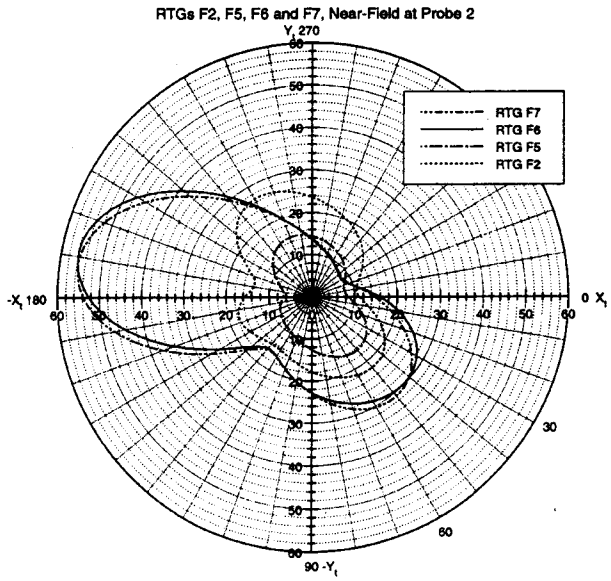

Figure 7

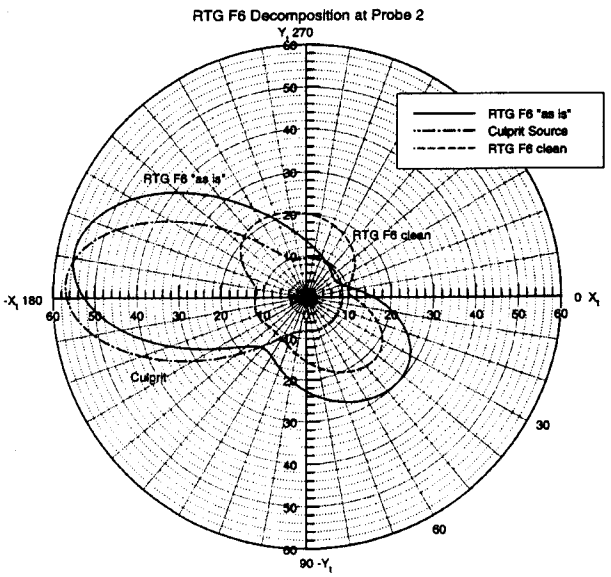

Figure 8

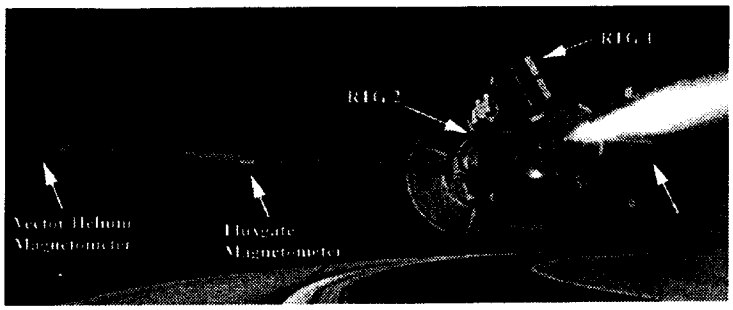

Figure 9

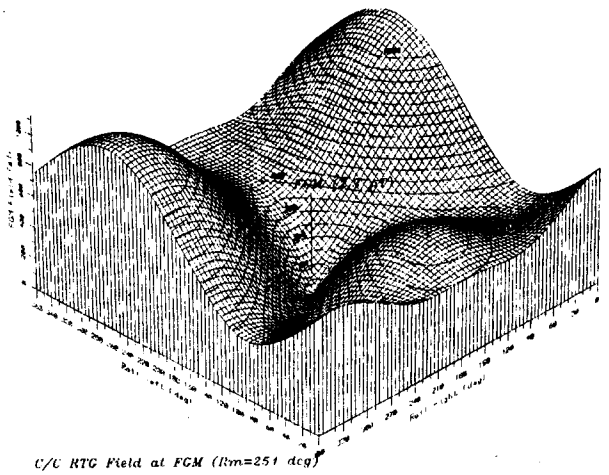

Figure 10

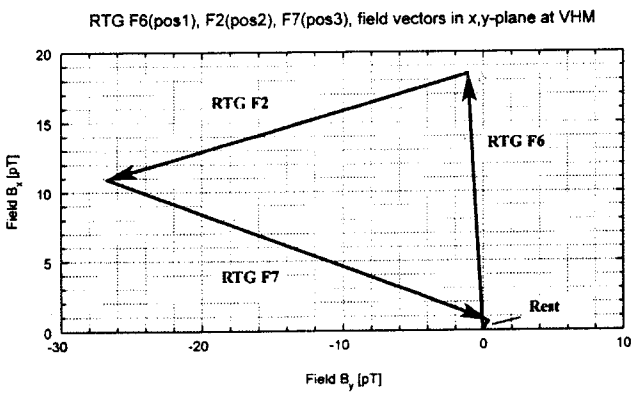

Figure 11

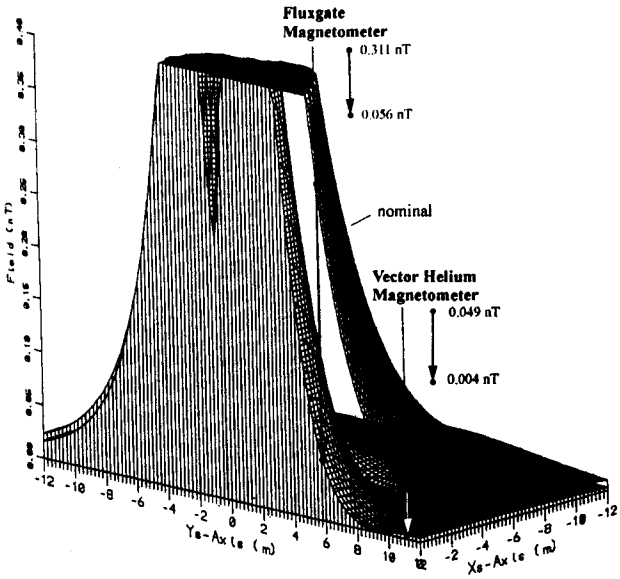

Figure 12

References

[1] Eichorn W L 1972, *Magnetic dipole moment determination by near field analysis*, NASA TN D-6685, July 1972.

[2] Neubauer F M 1974, *Theoretical and observational analysis of spacecraft fields*, J Geophys Res, April 1974.

[3] Polak E 1971, *Computational methods in optimization*, Academic Press.

[4] Mehlem K 1978, *Multiple magnetic dipole modeling and field prediction of satellites*, IEEE Trans on Magnetics, September 1978.

[5] Mehlem K 1989, *Ulysses RTG F3 magnetic compensation*, ESA/ESTEC Working Paper 1537, March 1989, to be obtained from the author.

[6] Mehlem K 1996, *Cassini RTG F5 magnetic analysis report*, ESA/ESTEC-JPL internal working paper, January 1996, to be obtained from the author.

[7] Mehlem K 1996, *Cassini RTG F2 magnetic analysis report*, ESA/ESTEC-JPL internal working paper, July 1996, to be obtained from the author.

[8] Mehlem K 1997, *Cassini RTG F7 magnetic analysis report*, ESA/ESTEC-JPL internal working paper, January 1997, to be obtained from the author.

[9] Mehlem K 1997, *Cassini RTG F6 magnetic analysis report*, ESA/ESTEC-JPL internal working paper, January 1997, to be obtained from the author.

[7] Mehlem K 1996, *Cassini RTG F2 magnetic analysis report*, ESA/ESTEC-JPL internal working paper, July 1996, to be obtained from the author.

[8] Mehlem K 1997, *Cassini RTG F7 magnetic analysis report*, ESA/ESTEC-JPL internal working paper, January 1997, to be obtained from the author.

[9] Mehlem K 1997, *Cassini RTG F6 magnetic analysis report*, ESA/ESTEC-JPL internal working paper, January 1997, to be obtained from the author.